East Asian Journal on Applied Mathematics
doi: 10.4208/eajam.010914.250315a

Vol. **5**, No. 2, pp. 138-149
May 2015

Computational Study of Nonadiabatic Wave Patterns in Smouldering Combustion under Microgravity

Ekeoma Rowland Ijioma[1,*], Hirofumi Izuhara[3], Masayasu Mimura[1,2] and Toshiyuki Ogawa[1,2]

[1] *Meiji Institute for Advanced Study of Mathematical Sciences, Meiji University, 4-21-1 Nakano, Nakano-ku, Tokyo, 164-8525, Japan.*
[2] *Graduate School of Advanced Mathematical Sciences, Meiji University, 4-21-1 Nakano, Nakano-ku, Tokyo, 164-8525, Japan.*
[3] *Faculty of Engineering, University of Miyazaki, 1-1 Gakuen Kibanadai-nishi, Miyazaki 889-2192, Japan.*

Received 1 September 2014; Accepted (in revised version) 25 March 2015

Abstract. We numerically study a thermal-diffusive model for smouldering combustion under microgravity with convective heat losses. In accordance with previous experimental observations, it is well known that porous materials burning against a gaseous oxidiser under microgravity exhibit various finger-like char patterns due to the destabilising effect of oxidiser transport. There is a close resemblance between the pattern-forming dynamics observed in the experiments with the mechanism of thermal-diffusive instability, similar to that occurring in low Lewis number premixtures. At large values of the Lewis number, the finger-like pattern coalesces and propagates as a stable front reminiscent of the pattern behaviour at large Péclet numbers in diffusion-limited systems. The significance of the order of the chemical kinetics for the coexistence of both upstream and downstream smoulder waves is also considered.

AMS subject classifications: 80A25, 35K57, 80A30, 35B36

Key words: Filtration combustion, smouldering, fingering instability, nonadiabatic, chemical kinetics.

1. Introduction

Smouldering combustion occurs in many domestic and technological processes. However, it can also be a potential fire hazard, and understanding the mechanism of smoulder wave propagation is important. We are presently interested in the structure of smoulder waves arising in microgravity environments, specifically aboard a spacecraft where fire safety measures are paramount. It is known that the structure of smoulder waves exhibits different finger-like patterns in microgravity experiments aboard spacecraft [15] and in

*Corresponding author. *Email addresses:* e.r.ijioma@gmail.com (E.R. Ijioma), hiro.izuhara@gmail.com (H. Izuhara), mimura.masayasu@gmail.com (M. Mimura), togw@meiji.ac.jp (T. Ogawa)

 ©2015 Global-Science Press

https://doi.org/10.4208/eajam.010914.250315a Published online by Cambridge University Press



(a) Connected (b) Tip-splitting (c) Sparse

Figure 1: Spatial profiles of two-dimensional fingering (char) patterns of a filter paper sample, observed experimentally in a Hele-Shaw cell; The char propagation is from bottom to top. Ignition is initiated at the bottom and oxidiser gas is passed from the top, in a typical counterflow configuration. The char is identified by the dark finger-like patterns, and the lighter shades are the quenched part of the flame that separates the regions of burned parts from unburned parts. (a) Connected front that occurs at high flux velocity, where the front is stable. (b) Tip-splitting regime marked by splitting of sole fingers at the tip, observed at moderate flux velocity. (c) Sparse fingers that appear at relatively low flux velocity, where the fingers are more distinct from each other and the tips do not split. The snapshots are courtesy of E. Moses (Weizmann Institute of Science).

quasi-two-dimensional Hele Shaw cells [20–22]. The fingering patterns differ from those observed in a natural convection dominated environment, and include distinct states that depend upon the velocity of a gaseous oxidiser. Thus although the oxidiser exerts a destabilising effect on the emerging smoulder waves, there are three steady states — viz. sparse, tip-splitting and connected front (cf. Fig. 1). The smoulder wave basically proceeds as a self-sustaining reaction front. This front propagates on the surface of a solid porous sample, which reacts with an oxidiser gas infiltrating its pores. The direction of flow of the gaseous oxidiser, relative to the direction of propagation of the reaction front, can be classified into distinct configurations of practical interest due to the characteristic features they exhibit. For a detailed discussion of distinct smouldering configurations, see Refs. [13, 14, 17, 18]. In this article, we focus on the smouldering regime referred to as reverse smoulder, where the direction of the gaseous oxidiser flow is opposite to the direction of the reaction front.

In order to understand the pattern-forming dynamics, various macroscopic models have been studied in different contexts. In Refs. [4, 8], a reaction-diffusion system was proposed to study the distinct fingering regimes based on the mechanism of diffusion-limited instability exhibited in the experimental observations reported [15, 20–22]. The diffusion-limited mechanism describes the destabilisation of the smoulder waves through the oxidiser velocity (or Péclet number in dimensionless systems), emphasising the effect of reactant transport on the propagating smoulder waves. Filtration combustion models have also been proposed [7, 10, 12]. However, in thermal-diffusive models the instability of propagating smoulder waves is easier to understand based on two competing transport processes — viz. the transport of reactants and the transport of heat. It is known that the transport of heat has a stabilising effect on the waves. There are various thermal-diffusive models in the literature, notably in the framework of premixed combustion, exhibiting similar qualitative behaviour to the observed situation in non-premixed flames. For instance, it

https://doi.org/10.4208/eajam.010914.250315a Published online by Cambridge University Press

was concluded that the diffusive-thermal instability of non-premixed flames occurs in a manner similar to that of premixed flames [3]. In dimensionless combustion systems, the mechanism of thermal-diffusive instability is usually characterised by the Lewis number — i.e. at large Lewis numbers the combustion wave stabilises. Furthermore, thermal-diffusive models have been investigated in our present context [3, 7, 9, 11, 19].

Here we extend the adiabatic model in Refs. [6, 7] via homogenisation theory for periodic structures, for a nonadiabatic situation with a convective heat transfer mechanism. For details of homogenisation theory, interested readers may refer to Refs. [1, 2, 5, 16]. We analyse the combustion wave behaviour in both one and two dimensions by direct numerical simulation of the dimensionless reaction-diffusion system, with a focus on the influence of the order of the chemical kinetics and the Lewis number. In Section 2, we describe the mathematical model and its rescaling, and our numerical solution schemes. Our one-dimensional and two-dimensional numerical results are presented in Section 3, and concluding remarks are made in Section 4.

2. Mathematical Model

In order to capture the pertinent physics for the phenomenon of interest, our proposed model has filtration properties that are akin to the influence of porous medium obstacles, convective heat transfer, and a one-step irreversible exothermic reaction with Arrhenius kinetics. The influence of the chemical kinetics is considered by a comparison with a second-order case. An appropriately non-dimensionalised set of equations for the temperature, concentration of gaseous oxidiser and the density of solid fuel (or char product) is then [7]

$$\begin{aligned} u_t &= u_{xx} + u_{yy} + \phi\Lambda Pe u_x + \beta\gamma f(u,v,w) - \tilde{h}(u-\sigma)\,, \\ \phi v_t &= Le^{-1}(v_{xx} + v_{yy}) + \phi Pe v_x - \gamma f(u,v,w)\,, \\ w_t &= -H_w \gamma f(u,v,w)\,, \end{aligned} \tag{2.1}$$

where the subscripts denote respective partial derivatives and $f(u,v,w)$ is the reaction rate function. The other notational details are: u is the nondimensional temperature in units of u_b, the adiabatic temperature of combustion products; v is the nondimensional concentration of the gaseous oxidiser in units of v_0, a reference inlet gaseous mixture; w is the density of solid fuel in units of w_0, initial density of the solid; x and y are the non dimensional spatial coordinates in units of $l_{th} = \alpha/U_b$, the thermal width of the flame, where α is the effective thermal diffusivity of the mixture and U_b is the speed of a planar adiabatic flame at infinitely large activation temperature $\theta = u_a/u_b$, with u_a, the dimensional activation temperature; t is the nondimensional time in units l_{th}/U_b; $\sigma = u_0/u_b$ is the nondimensional temperature of the surroundings; u^* is a ignition temperature; $\tilde{h}$ is the nondimensional heat transfer coefficient in units of $U_b c^{\text{eff}}/\phi^s l_{th}$, where c^{eff} is the effective volumetric heat capacity and ϕ^s is the surface fraction derived from homogenisation [7]; $H_w = v_0/\phi^s w_0$ is a nondimensional coefficient corresponding to the ratio of initial reactants species; ϕ is the system porosity; β is the nondimensional heat release in units of $c^{\text{eff}} u_b/v_0$; γ is the nondimensional pre-exponential factor in units of $U_b/\phi^s l_{th}\theta\exp(-\theta)$; $\Lambda = c_g/c^{\text{eff}}$ is the

https://doi.org/10.4208/eajam.010914.250315a Published online by Cambridge University Press

ratio of heat capacities, with c_g, heat capacity of the gaseous mixture; $Pe = Vl_{th}/\alpha$ is the Péclet number and $Le = \alpha/D^{\text{eff}}$ is the Lewis number, where V and D^{eff} are respectively the prescribed flow velocity and effective mass diffusivity of the gaseous phase. The reaction rate function

$$f(u,v,w) = \begin{cases} vw\theta \exp(\theta - \theta/u)\,, & \text{if } u \geq u^*\,, \\ 0\,, & \text{otherwise}\,, \end{cases} \tag{2.2}$$

describes a second-order kinetics — for comparison with the first-order Arrhenius law reactant consumption rate

$$f(u,v) = \begin{cases} v\theta \exp(\theta - \theta/u)\,, & \text{if } u \geq u^*\,, \\ 0\,, & \text{otherwise}\,, \end{cases} \tag{2.3}$$

when the kinetic equation in Eq. (2.1) describes the density of char — i.e. the solid product of combustion. (However, the sign of the right-hand side changes in this respect.) In one dimension, we consider a finite interval $0 < x < L_x$. In two dimensions, we consider a bounded rectangular domain $0 < x < L_x$, $0 < y < L_y$ with insulation conditions at the top and bottom boundaries — i.e.

$$u_y = v_y = 0 \;\text{ at } y = 0, L_y\,.$$

At the inlet end $x = L_x$ and the outlet end $x = 0$, the boundary conditions adopted are

$$(u_x, v_x)(t,0) = (0,0)\,, \qquad (u_x, v)(t, L_x) = (0, v_0)\,, \qquad t > 0\,, \tag{2.4}$$

corresponding to ignition initiated at the left boundary and the smoulder wave propagating from the left to the right boundary where the gaseous oxidiser is passed. This configuration describes a reverse combustion as previously mentioned, since the flow direction of the gaseous oxidiser is opposite to the propagation direction of the front. Finally, the problem is closed on assuming the initial conditions

$$(u,v,w)(0,x,y) = (u_0(x,y), v_0, w_0) \quad \text{for } 0 < x < L_x\,,\; 0 < y < L_y\,. \tag{2.5}$$

2.1. Numerical schemes

For the one-dimensional problem, we used the Method of Lines (MOL), which typically involves a finite difference spatial discretisation followed by a suitable time integration of the resulting ODE system. Thus let $h := L_x/N_x$ be the spatial step size, where $N_x > 0$ is the number of discretisation intervals. The interval $I = 0 < x < L_x$ can then be represented by a uniform grid of nodes $I_h := \{x_i := ih \in I \mid i = 0, \cdots, N_x\}$. We define a grid function $\mathscr{G}_h^I := \{\varphi_h \mid \varphi_h : I_h \to \mathbb{R}\}$ such that $\varphi_i(t) := \varphi_h(t, x_i)$, $\varphi_h \in C^1([0,T], \mathscr{G}_h^I)$, $T > 0$. The second-order derivatives were defined by the central difference discretisation $\triangle_h \varphi_i(t) := (\varphi_{i-1}(t) - 2\varphi(t) + \varphi_{i+1}(t))/h^2$, and the first-order derivatives by the forward difference discretisation $\nabla_h \varphi_i(t) := (\varphi_{i+1}(t) - \varphi_i(t))/h$, for $\varphi_h \in C^1([0,T], \mathscr{G}_h^I)$.

https://doi.org/10.4208/eajam.010914.250315a Published online by Cambridge University Press

Consequently, for $u_h \in C^1([0,T],\mathscr{G}_h^I)$, $v_h \in C^1([0,T],\mathscr{G}_h^I)$ and $w_h \in C^1([0,T],\mathscr{G}_h^I)$, the semi-discrete solution of the problem is the triple (u_h, v_h, w_h) defined by the system of ordinary differential equations for $t > 0$:

$$\begin{aligned}
&\frac{du_i(t)}{dt} = \triangle_h u_i(t) + \phi\Lambda Pe\nabla_h u_i(t) + \beta\gamma f\big(u_i(t), v_i(t), w_i(t)\big) - \tilde{h}\big(u_i(t)-\sigma\big),\ i = 0,\cdots,N_x\,,\\
&\phi\frac{dv_i(t)}{dt} = Le^{-1}\triangle_h v_i(t) + \phi Pe\nabla_h u_i(t) - \gamma f\big(u_i(t), v_i(t), w_i(t)\big)\,,\quad i = 0,\cdots,N_x-1\,,\\
&\frac{dw_i(t)}{dt} = -\gamma f\big(u_i(t), v_i(t), w_i(t)\big),\quad i = 0,\cdots,N_x\,,
\end{aligned} \tag{2.6}$$

subject to the initial conditions

$$u_i(0) = u_0(x_i)\,,\quad v_i(0) = v_0\,,\quad w_i(0) = w_0\,,\quad \text{for } i = 0,\cdots,N_x\,. \tag{2.7}$$

The boundary conditions at $i = 0, N_x$ have been implemented by eliminating the ghost nodes — i.e. nodes outside the grid points appearing in the end grid points of the first equation and the left end grid point of the second equation, using appropriate first-order difference approximations on the boundary conditions defined in Eq. (2.4). For Dirichlet boundary conditions, specifically for the variable v, we prescribe a boundary value at the right end grid point:

$$v_{N_x}(t) = v_0\,,\quad t > 0\,. \tag{2.8}$$

On the other hand, an explicit finite difference scheme on a uniform orthogonal grid will be employed for a two-dimensional problem.

3. Numerical Results

In this section, we present our numerical results for the model in Section 2 using the methods described above. The numerical integration for the one-dimensional problem was achieved with a variable order ODE solver in Matlab®. The parameter values used in the numerical simulation are given in Table 1, unless otherwise stated. In all numerical simulations, the spatial domain length is $L_x = 200$. The Péclet and Lewis numbers are taken as free parameters with assumed values according to the physical problem of interest.

Table 1: Typical set of parameter values used in the numerical simulation.

θ	β	γ	$\tilde{h}$	ϕ	v_0	w_0	σ	Λ	H_w	u^*
1.94	20.	5.0	0.28	0.497	0.1	1.0	0.02	0.0	1.0	0.1

https://doi.org/10.4208/eajam.010914.250315a Published online by Cambridge University Press

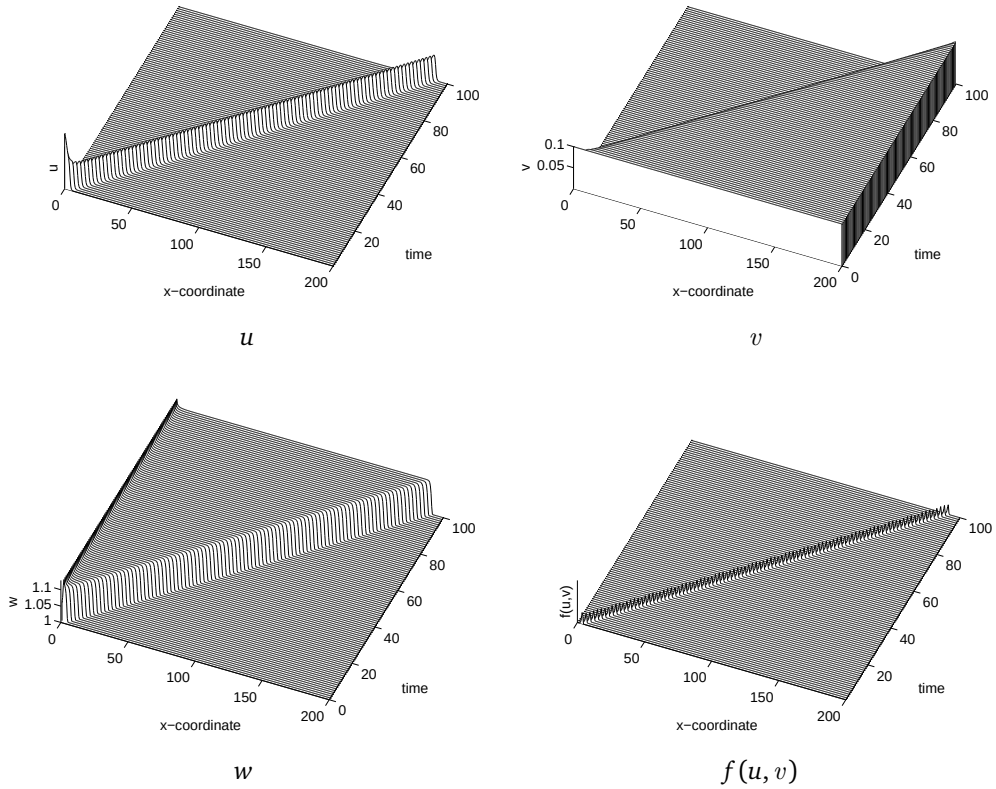


Figure 2: Spatio-temporal profiles of u, v, w and the heat release rate f, from model (3.1) with a first-order kinetics. The parameters used in the simulation are taken from Table 1. In this case, $Pe = 2.0$ and $Le = 0.25$.

3.1. One-dimensional combustion waves

We first consider a one-dimensional minimal model

$$\begin{aligned} u_t &= u_{xx} + \phi\Lambda Pe u_x + \beta\gamma f(u,v) - \tilde{h}(u-\sigma)\,, \\ \phi v_t &= Le^{-1} v_{xx} + \phi Pe v_x - \gamma f(u,v)\,, \\ w_t &= H_w \gamma f(u,v)\,. \end{aligned} \tag{3.1}$$

An obvious difference between this model and the diffusion-limited model presented in Ref. [4, 8] is that the diffusion term of v in the second equation has been scaled with the reciprocal of Le. For the present simulation, we also assume that the reaction rate has first-order kinetics according to Eq. (2.3). Fig. 2 depicts the travelling wave profile. In this case, the waves are not reflected downstream on reaching the end of the line at $L_x = 200$, because the order of the chemical kinetics excludes a contribution from the solid fuel consumption.

Next, we replace the kinetic term in the model (3.1) with the second-order kinetics described by Eq. (2.2). The simulation in this case exhibits a reflection of the thermal front

https://doi.org/10.4208/eajam.010914.250315a Published online by Cambridge University Press

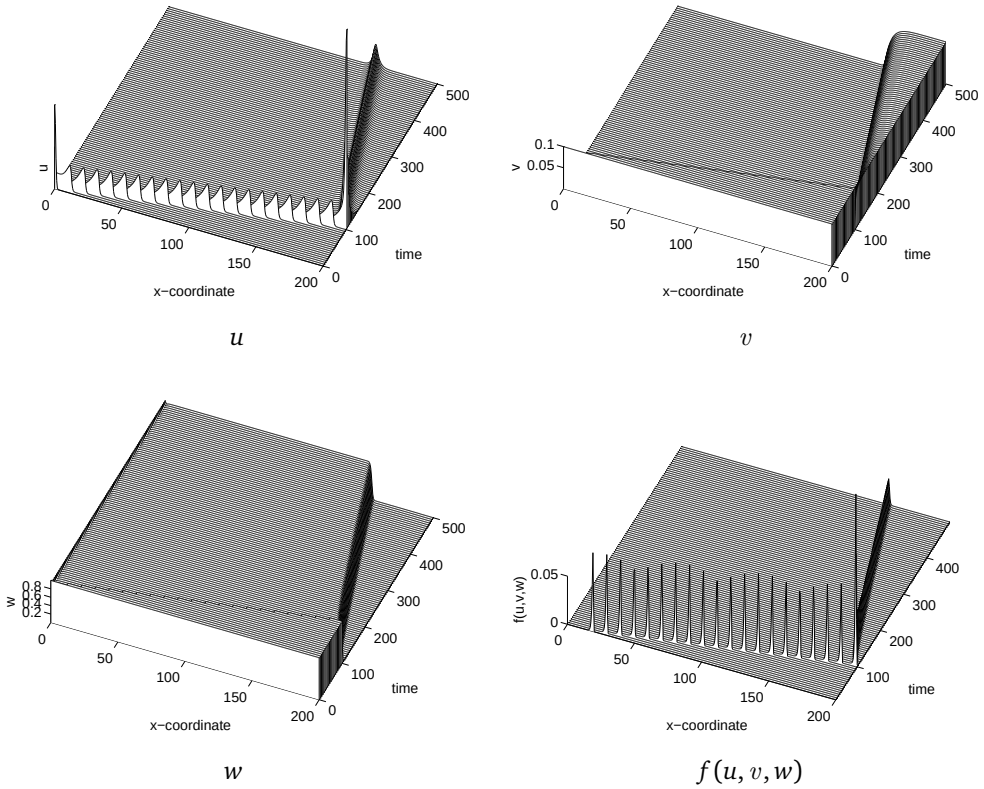


Figure 3: Spatio-temporal profiles of u, v, w and the heat release rate f, from model (3.1) with a second-order kinetics. The parameters used in the simulation are taken from Table 1. In this case, $Pe = 2.0$ and $Le = 0.25$.

of u as depicted in Fig. 3 — i.e. the smoulder waves are reflected on reaching the end of the line. This downstream phenomenon for smoulder waves was reported in microgravity experiments [15]. Thus we see the importance of a second-order kinetics, where the waves turn back downstream on including solid fuel consumption in the chemical model. Fig. 4 shows that the structure of the travelling waves moves upstream until the end of the domain at $L_x = 200$, and that after about $t = 200$ it is no longer reflected downstream. For Pe fixed within a critical range (e.g. $Pe = 0.35$) and increasing values of Le the smoulder wave is not reflected downstream, indicating that high heat diffusivity inhibits the propagation of the downstream smoulder provided that the Pe value remains within a certain range.

3.2. Two-dimensional fingering instability

In one dimension, we found the wave behaviour depends on the chemical kinetics and that there are limiting values of the Péclet and Lewis numbers. Thus the one-dimensional waves propagate only at relatively large Pe number, and large Le numbers can quench the

https://doi.org/10.4208/eajam.010914.250315a Published online by Cambridge University Press

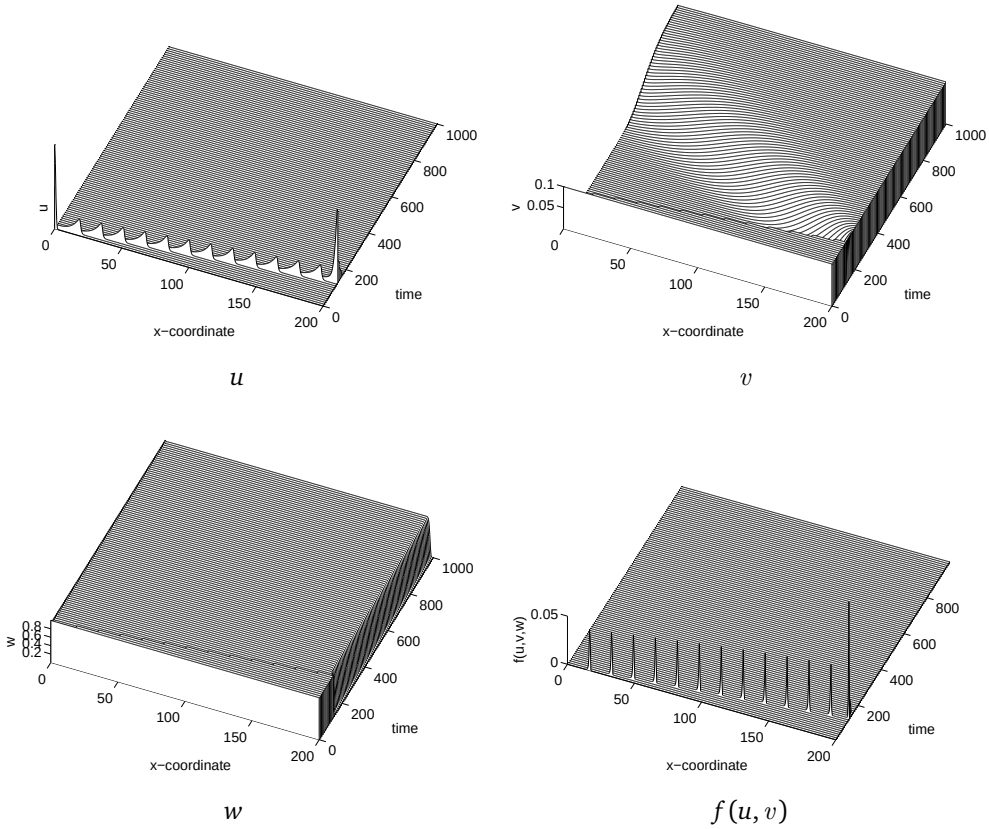


Figure 4: Spatio-temporal profiles of u, v, w and the heat release rate f, for the model (3.1) with second-order kinetics. The parameters used in the simulation are taken from Table 1. In this case, $Pe = 0.35$ and $Le = 1.5$.

propagation downstream. However, there are other interesting phenomena under microgravity environments to consider at higher dimensions.

In this section, we numerically investigate the fingering instability mechanism under microgravity from the point of view of the proposed thermal-diffusive model (2.1). From the one-dimensional results of the previous section, we expect that at large Lewis numbers and within a critical range of Péclet numbers the downstream smoulder waves are not viable. In addition, the system stabilises at increasing values of Le, and at large Péclet numbers, the fingering behaviour vanishes so there is a stable planar front. Furthermore, given the experimental observations [20–22] we expect that distinct fingering regimes are manifest in the thermal-diffusive model, in verifying the close resemblance of the pattern-forming dynamics with the diffusional instability reported in the experiments. We restrict our discussion here to the case of a second-order kinetic law, but we also envisage that the results of the one-dimensional problem with first-order kinetics applies in the two-dimensional case. Here, we consider the problem in Section 2 over a rectangular domain

https://doi.org/10.4208/eajam.010914.250315a Published online by Cambridge University Press

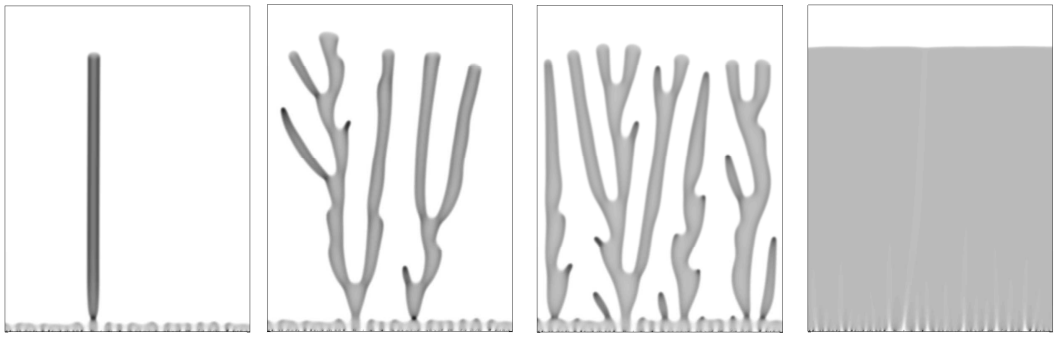


Figure 5: Collage of char patterns of w as a function of Pe and for $Le = 0.5$. (a) $Pe = 0.16$ (sparse finger); (b) $Pe = 0.27$; (c) $Pe = 0.35$ (tip-split fingers); (d) $Pe = 4.0$; (connected front). The pattern behaviour describes the limit of large Péclet numbers in the thermal-diffusive model (2.1); Similar results can be realised from the point of view of diffusion-limited systems [8]. Here, ignition is initiated from the bottom, the gaseous oxidiser is passed from the top, and the smoulder front propagates from bottom to top. The dark shades represent the burned (charred) region, and the light shades the unburned region.

with $L_x = 200$ and $L_y = 150$.

3.2.1. Distinct fingering regimes

The system (2.1) was first controlled by varying the Pe number, while other parameters remain fixed. In particular, the adopted value of the Lewis number was $Le = 0.5$. Fig. 5 shows distinct fingering states, depending on the Pe number. In Fig. 5(a), the pattern exhibits a sole finger of constant width that propagates from bottom to top, corresponding to $Pe = 0.16$. As Pe is increased, the density of fingers increases and the fingers begin to tip-split, but remain distinct from each other — cf. Fig. 5(b) and Fig. 5(c). The results in Fig. 5(d) for even higher values of Pe show a stable planar front occurring at $Pe = 4.0$. At this point, the simulation exhibits the diffusional instability mechanism in the system, consistent with that reported in Ref. [15, 21]. This instability arises when the transport of the reactants (the oxidiser transport in this case) is limited. It can also be shown that two-dimensional travelling front solutions exist for the results depicted in Figs. 5(a) and (d).

3.2.2. Lewis number effects

Next, the system (2.1) was controlled by varying the Le number, while other parameters remained fixed. In particular, the Péclet number $Pe = 0.35$ was adopted, as in the one-dimensional simulation of Section 3.1. Fig. 6 shows the evolution of the fingering patterns for various values of the Lewis number. Thus for $Pe = 0.35$ and increasing Le number up to $Le = 1.5$, initially sparse fingers shown in Fig. 6(a) gradually transit into a stable planar solution regime — i.e. the system stabilises at sufficiently large values of the Lewis number, when the finger-like patterns vanish. This result is consistent with the linear stability results

https://doi.org/10.4208/eajam.010914.250315a Published online by Cambridge University Press

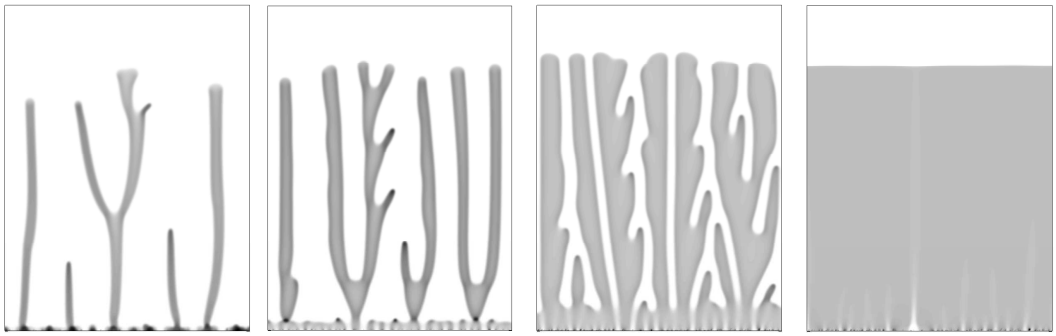


Figure 6: Collage of char patterns of w as a function of Le and for $Pe = 0.35$. (a) $Le = 0.2$; (b) $Le = 0.4$; (c) $Le = 0.8$; (d) $Le = 1.5$. The pattern behaviour describes the limit of large Lewis numbers in the thermal-diffusive model (2.1).

reported Ref. [19] for nonadiabatic reverse smoulder waves. We also point out that the wave in Fig. 6(d) is not reflected on reaching the edge of the domain, similar to the one-dimensional behaviour of the travelling waves — cf. Fig. 4.

4. Conclusions

A simple thermal-diffusive model with convective heat transfer predicts the fingering instability arising in smouldering combustion under microgravity. In comparison with phenomenological RD models [4, 8] and most other combustion models that neglect the influence of porous media obstacle [19], the strength of the convective flux in the proposed model (2.1) derived by homogenisation is limited by the presence of nonunity porosity. However, within an appropriately chosen parameter space the two modelling approaches are functionally identical.

In one dimension, the order of the chemical kinetics was found to be significant for the viability of downstream smoulder waves. The smoulder waves turned downstream when a second-order kinetics was invoked. Within a critical range of Péclet numbers and at large Lewis numbers (say $Le \geq 1$), the downstream smoulder waves were no longer viable — i.e. the smoulder waves no longer occur. Thus for suitable fixed Pe values, increasing the Le number stabilises the reverse combustion, inhibiting the propagation of forward combustion in the absence of convective dominance in the system. It is notable that the extinction limit observed in the one-dimensional results cannot be extended by the thermal-diffusive effects of the Le number if the Pe number increases beyond a certain threshold [3].

In two dimensions, we verified the results of our one-dimensional simulations of the limiting values of the Lewis and Péclet numbers. The dynamics of the pattern behaviour exhibited by the proposed thermal-diffusive model (2.1) is reminiscent of the diffusion-limited instability reported in [21], and similar to the pattern dynamics reported from other diffusion-limited models [4, 8, 12].

https://doi.org/10.4208/eajam.010914.250315a Published online by Cambridge University Press

Acknowledgments

This work is supported by the Meiji Institute for Advanced Study of the Mathematical Sciences (MIMS), Center for Mathematical Modeling and Applications (CMMA).

References

[1] N. Bakhvalov and G. Panasenko, *Homogenisation: Averaging Processes in Periodic Media*, volume 36 of Mathematics and Its Applications (Soviet Series), Kluwer Academic Publishers Group, Dordrecht (1989).

[2] A. Bensoussan, J.L. Lions, and G. Papanicolaou, *Asymptotic Analysis for Periodic Structures*, volume 5 of Studies in Mathematics and Its Application, North-Holland (1978).

[3] R.H. Chen, G.B. Mitchell, and P.D. Ronney, Diffusive-thermal instability and flame extinction in nonpremixed combustion, in *Symposium (International) on Combustion*, volume 24, pp. 213–221, Elsevier (1992).

[4] A. Fasano, M. Mimura, and M. Primicerio, *Modelling a slow smoldering combustion process*, Math. Methods Appl. Sci. **33**, 1211–1220 (2009).

[5] U. Hornung, *Homogenization and Porous Media*, volume 6 of Interdisciplinary Applied Mathematics, Springer-Verlag, New York (1997).

[6] E.R. Ijioma, *Homogenization approach to filtration combustion of reactive porous materials: Modeling, simulation and analysis*, PhD thesis, Meiji University, Tokyo, Japan (2014).

[7] E.R. Ijioma, A. Muntean, and T. Ogawa, *Pattern formation in reverse smouldering combustion: A homogenisation approach*, Combust. Theory Model. **17**(2), 185–223 (2013).

[8] K. Ikeda and M. Mimura, *Mathematical treatment of a model for smoldering combustion*, Hiroshima Math. J. **38**, 349–361 (2008).

[9] L. Kagan and G. Sivashinsky, *Incomplete combustion in nonadiabatic premixed gas flames*, Phys. Rev. E. **53**, 6021–6027 (1996).

[10] L. Kagan and G. Sivashinsky, *Pattern formation in flame spread over thin solid fuels*, Combust. Theory Model. **12**, 269–281 (2008).

[11] J.S. Kim, F.A. Williams, and P.D. Ronney, *Diffusional-thermal instability of diffusion flames*, J. Fluid Mech. **327**(1), 273–301 (1996).

[12] C. Lu and Y.C. Yortsos, *Pattern formation in reverse filtration combustion*, Phys. Rev. E. **72**, 036201(1–16) (2005).

[13] T. Ohlemiller and D. Lucca, *An experimental comparison of forward and reverse smolder propagation in permeable fuel bed*, Combust. Flame **54**, 131–147 (1983).

[14] T.J. Ohlemiller, *Modeling of smoldering combustion propagation*, Progress in Energy Combust. Sci. **11**, 277–310 (1985).

[15] S.L. Olson, H.R. Baum, and T. Kashiwagi, *Finger-like smoldering over thin cellulose sheets in microgravity*, Twenty-Seventh Symposium (International) on Combustion, pp. 2525–2533 (1998).

[16] E. Sanchez-Palencia and A. Zaoui, *Homogenization Techniques for Composite Media*, volume 272 of Lecture Notes in Physics, Springer (1985).

[17] D.A. Schult, B.J. Matkowsky, V.A. Volpert, and A.C. Fernandez-Pello, *Propagation and extinction of forced opposed smolder waves*, Combust. Flame **101**, 471–490 (1995).

[18] C.W. Wahle, B.J. Matkowsky, and A.P. Aldushin, *Effects of gas-solid nonequilibrium in filtration combustion*, Combust. Sci. Tech. **175**, 1389–1499 (2003).

[19] F.P. Yuan and Z.B. Lu, *Structure and stability of non-adiabatic reverse smolder waves*, Appl. Math. Mech. **34**(6), 657–668 (2013).

https://doi.org/10.4208/eajam.010914.250315a Published online by Cambridge University Press

[20] O. Zik and E. Moses, *Fingering instability in combustion: The characteristic scales of the developed state*, Proceeding of Combustion Institute **27**, 2815–2820 (1998).
[21] O. Zik and E. Moses, *Fingering instability in combustion: An extended view*, Amer. Phys. Soc. **60**, 518–531 (1999).
[22] O. Zik, Z. Olami, and E. Moses. *Fingering instability in combustion*, Phys. Rev. Lett. **81**, 3868–3871 (1998).

https://doi.org/10.4208/eajam.010914.250315a Published online by Cambridge University Press